Eur. Phys. J. A **34**, 325–339 (2007)
DOI 10.1140/epja/i2007-10504-5

THE EUROPEAN PHYSICAL JOURNAL A

Regular Article – Theoretical Physics

Angular anisotropy of the fusion-fission and quasifission fragments

A.K. Nasirov[1,2,a], A.I. Muminov[2], R.K. Utamuratov[2], G. Fazio[3], G. Giardina[3], F. Hanappe[4], G. Mandaglio[3], M. Manganaro[3], and W. Scheid[5]

[1] Flerov Laboratory of Nuclear Reactions, JINR, 141980 Dubna, Russia
[2] Heavy Ion Physics Department, Institute of Nuclear Physics, 100214, Tashkent, Uzbekistan
[3] INFN, Sezione di Catania, and Dipartimento di Fisica dell'Università di Messina, 98166 Messina, Italy
[4] Université Libre de Bruxelles, 1050 Bruxelles, Belgium
[5] Institut für Theoretische Physik der Justus-Liebig-Universität, 35392, Giessen, Germany

Received: 15 May 2007 / Revised: 20 November 2007
Published online: 8 January 2008 –
Communicated by T.S. Bíró

Abstract. The anisotropy in the angular distribution of the fusion-fission and quasifission fragments for the $^{16}O + ^{238}U$, $^{19}F + ^{208}Pb$ and $^{32}S + ^{208}Pb$ reactions is studied by analyzing the angular-momentum distributions of the dinuclear system and compound nucleus which are formed after capture and complete fusion, respectively. The orientation angles of the axial symmetry axes of the colliding nuclei relative to the beam direction are taken into account for the calculation of the variance of the projection of the total spin onto the fission axis. It is shown that there is a large contribution of the quasifission fragments in the $^{32}S + ^{208}Pb$ reaction to the deviation of the experimental angular anisotropy from the statistical model results. Enhancement of anisotropy at low energies in the $^{16}O + ^{238}U$ reaction is connected with the quasifission of the dinuclear system having low temperature and relatively small effective moment of inertia.

PACS. 25.70.Jj Fusion and fusion-fission reactions – 25.70.Lm Strongly damped collisions – 25.85.Ge Charged-particle-induced fission

1 Introduction

The study of the mechanism of the fusion-fission process in the reactions with massive nuclei is of interest for both experimentalists and theorists to obtain a favorable way for the synthesis of superheavy elements or exotic nuclei far from the stability line. The last experiments on the synthesis of superheavy elements $Z = 114$, 115, 116 and 118 were successful at beam energies corresponding to 35–40 MeV excitation energies of the compound nucleus which is higher enough than the Bass barrier. The deformed actinide nuclei were used as targets in the synthesis of new superheavy nuclei in the $^{48}Ca + ^{238}U$, ^{244}Pu, ^{248}Cm reactions [1]. This means that the orientation angle of the symmetry axis of the target nucleus relative to the beam direction affects the fusion-fission mechanism. The cross-sections of events corresponding to the synthesis of superheavy elements are not higher than few picobarns [1] and the width of the evaporation residues excitation function is very narrow. At the same time the measured cross-sections of the fission fragments are several tens of millibarn [2] and the excitation function of fission fragments yields is very wide. This means that only a very small part of collisions in the narrow range of the beam energy leads to the formation of the evaporation residues considered as superheavy elements. The problem is to establish this small range of the beam energy as the optimal condition for the synthesis of superheavies. The main reason leading to the small values of the evaporation residue cross-sections seems to be connected with the small survival probability W_{sur} of the heated compound nucleus against fission by evaporating neutrons. It is well known that the W_{sur} decreases by an increase of the excitation energy E^*_{CN} and angular momentum ℓ_{CN} of the compound nucleus [3].

But the formation of the compound nucleus in reactions with massive nuclei has a hindrance: not all of the dinuclear systems formed at capture of the projectile by the target nucleus can be transformed into compound nuclei. We should stress that the estimation of the formation

[a] e-mail: nasirov@jinr.ru

probability is difficult by both experimental and theoretical methods. The determination of the fusion probability from the experimental data is ambiguous due to the difficulties to identify pure fission fragments of the splitting compound nucleus from the fragments which are formed in other processes of heavy-ion collisions like fast-fission, quasifission and deep inelastic collisions. By the way, the restoration of its value from the cross-sections of evaporation residues is model dependent. As a result there is a field for speculations which can be clarified indirectly by the analysis of the physical results connected with the formation of the compound nucleus. The angular distribution of reaction fragments is one of the informative quantity allowing us to study the fusion-fission mechanism of heavy-ion collisions. The study of correlations between mass and angular distribution of fragments of full momentum transfer reactions allows us to separate the pure fission fragments of the compound nucleus with a compact shape [4]. The mass and angular-momentum distributions of the reaction fragments are determined by the dynamics of collision. The complete kinetic energy relaxation (capture stage) is a main characteristic of the quasifission reactions. This means that quasifission takes place only after the capture of the projectile by the target nucleus. The mass equilibrium can be reached or not in dependence on the masses and mass asymmetry of the reactants [5], as well as on the dynamics of collision.

The goal of the present paper is to show the ability of the method based on the dinuclear-system (DNS) concept to calculate the angular-momentum distribution for the fusion-fission and quasifission fragments by analyzing the anisotropy of the angular distribution of both fusion-fission and quasifission fragments in reactions with deformed and nearly spherical target nuclei. Quasifission produces fragments like the fission fragments thus confusing the estimation of the fusion cross-section. In the quasifission process, the compound-nucleus stage is not reached.

In our model we calculate dynamically only the capture stage of the reaction. The second stage is the competition between complete fusion and quasifission in the evolution of the dinuclear system. We consider this stage by the statistical method based on the assumptions that in the relatively long-lived dinuclear system the thermal equilibrium is reached after the complete transformation of the relative kinetic energy into the excitation energy of the intrinsic and surface vibration degrees of freedom. It is assumed that the equilibrium of mass asymmetry degrees of freedom is reached. The mass distribution strongly depends on the potential energy surface. From the theoretical analysis of the fusion-fission and quasifission reactions it is known that the reaction time of the fusion-fission process is sufficiently longer than the one of quasifission. The competition between these processes takes place after the capture of nuclei has occurred. The capture stage can be analyzed with the diabatic potential because its time is about 5–7 10^{-22} s. But the competition between fusion-fission and quasifission processes can take place during short or longer times in dependence on the beam energy and orbital angular momentum, as well as on how massive are the colliding nuclei. The short-time competitions between quasifission and fusion can be investigated by the diabatic potential. For the long-time competitions we deal with a potential which is intermediate between the diabatic and the adiabatic one. The reactions considered in our paper have large mass asymmetry. Therefore, in the analysis of these reactions we deal with the short-time competitions between quasifission and complete fusion. So, the use of the diabatic potential in our analysis is not in contradiction with the physical picture of the process. For example, this kind of conclusions was made in ref. [6] where the author discussed the use of the diabatic and adiabatic potentials in the study of quasifission in a heavy fusing system.

The partial capture, fusion and quasifission excitation functions, as well as the corresponding mean square values of the angular momentum calculated in this work were used to determine the anisotropy A of the fragment angular distribution by formula (1) as a function of the spin distribution of the fissioning systems: compound nucleus and dinuclear system. The results were compared with the experimental data for the observed anisotropy A of the angular distributions of fragments of the $^{16}\mathrm{O} + ^{238}\mathrm{U}$ [7], $^{19}\mathrm{F} + ^{208}\mathrm{Pb}$ [8] and $^{32}\mathrm{S} + ^{208}\mathrm{Pb}$ [5,9] reactions. It was shown that the large anisotropy of in the angular distribution of fragments of the full momentum transfer events in the $^{16}\mathrm{O} + ^{238}\mathrm{U}$ [7] reaction at the lowest beam energies is connected to the contribution of the quasifission products. The contribution of the latter process is dominant in the $^{32}\mathrm{S} + ^{208}\mathrm{Pb}$ [5,9] reaction for all the beam energy range and this causes the large anisotropy in the measured angular distribution of the fragments.

We present also the results obtained by an alternative way of estimation of the angular anisotropy of the quasifission products A_{qf}. A_{qf} is estimated from the angular distribution of the quasifission products. The rotation angle of the dinuclear system is found as the sum of the rotation angles during capture and before its break-up for the given initial values of the beam energy and orbital angular momentum ℓ_0. The former angle is found by solving the equation of motions for capture and the latter angle is estimated by the product of the angular velocity and decay time of the dinuclear system.

The paper is organized in the following way. In sect. 2, we discuss the possibility to use the anisotropy of the angular distribution of fragments to establish their origination. In sect. 3 we present the method to calculate the orbital angular-momentum distribution, mean square values $\langle \ell^2 \rangle$, and anisotropy A of the angular distribution of the fission and quasifission fragments. A short presentation about how we calculate capture, fusion, and quasifission excitation functions is given in sect. 4. The results of the anisotropy of the fragment angular distribution of the fission and quasifission fragments are presented and discussed in sect. 5. In sect. 6, we present an alternative way to calculate the angular anisotropy making use of the rotational angle and partial quasifission cross-sections. Conclusions are given in sect. 7.

2 About the interpretation of the anisotropy of the angular distribution of reaction fragments

The symmetric mass distributions at all angles and symmetric angular distributions relative to $\theta_{c.m.} = 90^\circ$ are characteristic features for the fission decay of a completely fused system. The angular distributions of fission fragments are often characterized by the ratio of the yield at 0° (or 180°) to the one at 90°, *i.e.*, $A = W(0^\circ)/W(90^\circ)$. The angular distribution of the fission products is described in the framework of the standard statistical model (SSM) usually making use of the fact that the fission saddle point configuration can be treated as a transition state between the compound system in its quasiequilibrium state and the two separated fission fragments [10]. This model is used under the assumption that the final direction of fragments is given by the orientation of the nuclear symmetry axis as the nucleus passes over the fission saddle point. This assumption may not be justified for the heaviest systems for which the saddle and scission point configurations have very different shapes. Consequently, in such case, the SSM may not properly describe the angular anisotropy of pure fission fragments in reactions with massive nuclei. Certainly, the discrepancy between theoretical and experimental estimations of the angular anisotropy is caused by an imperfection of the SSM and the experimental difficulties of separating the pure fission fragments. Calculations within the SSM assume the availability of a realistic spin distribution of the fissioning system. In turn the calculation of the spin distribution of the compound nucleus formed in the heavy-ion–induced reactions is a complicated task. The extraction of a realistic spin distribution from the measured angular distribution of reaction fragments may be ambiguous due to a sufficient contribution of quasifission. The authors of ref. [8] analyzing the experimental data determine the fission cross-sections by fitting the measured angular distributions of the fission fragments. To generate the angular-momentum distributions required to predict the shape of the fission angular distributions, approximate fusion cross-sections are used. In this paper, the "restored" fission angular distributions were used again and fitted to the measured data for the $^{19}\mathrm{F} + {}^{208}\mathrm{Pb}$ reactions. From the final fits the anisotropies A and the fusion-fission cross-sections as well as the value of K_0^2 at each bombarding energy were determined. In such an analysis, it was implicitly assumed that K_0^2 is independent of the total spin J. The reason of the failure of the statistical model to reproduce the measured data was considered doubtful for the application of the SSM at high energies when it was no longer valid if the fission barrier could be passed at the first attempt. This deviation occurs at large values of angular momenta where the fission barrier height is less than the saddle point temperature ($T \approx 1.6\,\mathrm{MeV}$). This means that all the properties of the fission process should be determined completely by the dynamics of the motion over the potential energy surface (PES). The role of the quasifission process was not discussed in [8].

So, there are three main points of view to interpret the experimentally observed angular anisotropy A: 1) authors of refs. [5,7] and we, in the present paper, explain it with the contribution of the quasifission process competing with the formation of the compound nucleus; 2) authors of ref. [11] observe a strict evidence of the anisotropy A, explaining such an anomaly by a new version of the pre-equilibrium fission model [12]; 3) the use of the scission point as the transition state was considered by the authors of refs. [13–15].

In ref. [7], the fission fragment anisotropies and mass distributions were measured over a wide range of angles for the $^{16}\mathrm{O} + {}^{238}\mathrm{U}$ reaction. The authors concluded that a systematic deviation of the measured fission fragment anisotropies from the transition state model predictions confirms the validity of the correlating anomalously large anisotropies with the presence of quasifission, particularly, at the lowest beam energies. In refs. [5,9], the sensitivity of the features of fission fragment angular distributions to nonequilibrium processes such as quasifission was shown by a quantitative analysis of the angular distributions of near-symmetric masses produced in the $^{32}\mathrm{S} + {}^{208}\mathrm{Pb}$ reaction.

The models which reproduce the fusion-fission excitation functions fail to account for the fission fragment angular-distribution data. The reasons of the failure could be connected with the effects of the entrance channel (presence of quasifission) or the fission exit channel (K-equilibrium is not reached, where K is the projection of the total spin of the nucleus on its axial symmetry axis) [16,17]. Certainly effects of both the abovementioned phenomena should be analyzed with the increase of the anisotropy A in the angular distribution of the reaction fragments. Vopkapic and Ivanisevic in ref. [17] suggested that at sub-barrier energies, fusion of projectile occurs only when the prolate deformed target is oriented in the beam direction, producing a narrow initial K distribution peaked around $K = 0$. The K equilibration time was also assumed to be not too short in comparison to the fission time. The use of a time-dependent and narrow K distribution in comparison to predictions of the statistical saddle point model could be envisaged and the fragment angular anisotropy could be explained.

The measured fission data corresponding to large values of the fragment angular anisotropy A can include a contribution of quasifission fragments leading to higher anisotropy than the ones predicted by standard statistical models [5,8], since at quasifission the dinuclear system never becomes as compact to be the compound nucleus, and also the K equilibration is probably not attained. The experimental data (see, for example, ref. [18]) confirm events with characteristic features, particularly in association with projectiles heavier than $^{24}\mathrm{Mg}$.

The possible roles of saddle point and scission point configurations were explored in ref. [14]. The analysis of the empirical correlations between the effective moments of inertia, the spin and Z^2/A of the compound nucleus allowed the authors of [14] to conclude that the observed anisotropies are between the predictions of the saddle

point and scission point transition state models. The authors of ref. [15] assumed the statistical equilibrium for the tilting mode at the pre-scission point, *i.e.* at a stage prior to the final split. They improved the statistical scission point transition state model by including the effects arising from the excitation of wriggling and twisting modes to reach a better agreement with experimental data. In the recent paper by Karpov *et al.* [19], the dynamical model of the calculation of the fission fragment angular distributions [20,21] was generalized to the case of the three-dimensional Langevin model. This model uses as an important parameter the relaxation time of the tilting mode. From fits of the experimental data on the fission fragment distribution of heavy fissioning compound systems, a K equilibration time of 4×10^{-21} was deduced.

So, the problem of the theoretical analysis of the measured angular anisotropy is that due to difficulties of separation of the products of the compound-nucleus fission from the quasifission products: the mixed experimental data have to be considered as the pure fission of the excited compound nucleus. Moreover, for the description of the pure fission of the excited compound nucleus with large excitation energy and angular momentum we need to improve the statistical scission point transition state model by including the effects arising from the excitation of wriggling and twisting modes (as in ref. [15]) or the new version of the pre-equilibrium fission model [12].

We consider the role of the entrance channel, namely quasifission events, in the observed angular anisotropy. The mean square values $\langle \ell^2 \rangle$ *versus* $E_{c.m.}$ for quasifission and complete fusion reactions are determined. We compare our results of A for quasifission and fusion-fusion products with the available estimations extracted from the experimental data [5,8].

3 Calculation of the anisotropy and mean square values $\langle \ell^2 \rangle$ of the angular distribution

The angular distribution of splitting fragments of the rotating system is determined by its angular-momentum distribution, namely, by the projection, K, of the total spin vector, J, onto the center axis of the separated fission fragments and by the moment of inertia of the fissioning system. The total spin has no component along the beam axis ($M = 0$), if the fissioning system is formed at capture (full momentum transfer) of a spinless projectile by a spinless target. We calculate the anisotropy A using our results of the angular-momentum distributions $\langle \ell^2 \rangle$ for the complete fusion and quasifission, and $\mathcal{J}_{eff}$ for the compound nucleus is found by the rotating finite-range model (RFRM) by Sierk [22] and for the DNS is determined by our model taking into account different mutual orientations of the symmetry axes of the interacting nuclei. Then, we can use the expression for the approximated anisotropy of the fission fragment angular distribution suggested by Halpern and Strutinski in ref. [23] and Griffin in ref. [24]:

$$A \approx 1 + \frac{\langle \ell^2 \rangle_{fus} \hbar^2}{4 \langle \mathcal{J}_{eff} T_{sad} \rangle}, \tag{1}$$

where

$$\frac{1}{\mathcal{J}_{eff}} = \frac{1}{\mathcal{J}_{\parallel}} - \frac{1}{\mathcal{J}_{\perp}} \tag{2}$$

is the effective moment of inertia on the saddle point for the compound nucleus; $\mathcal{J}_{\parallel}$ and $\mathcal{J}_{\perp}$ are moments of inertia around the symmetry axis and a perpendicular axis, respectively. Their values are determined in the framework of the RFRM by Sierk [22]. $\mathcal{J}_{eff}$ and T_{sad} are functions of $\langle \ell \rangle$ and their values for a given beam energy and orbital angular momentum are found by averaging $\langle \mathcal{J}_{eff} T_{sad} \rangle$ by the partial fusion cross-sections, similar as in formula (3).

The mean square values of the orbital angular momentum for the fusion-fission $\langle \ell^2 \rangle_{fus}$ and quasifission $\langle \ell^2 \rangle_{qf}$ processes are calculated by using the partial cross-sections of fusion, $\sigma_{fus}^{(\ell)}$, and quasifission, $\sigma_{qf}^{(\ell)}$, respectively. The above-mentioned mean square values are found by averaging over all orientation angles of the symmetry axis of deformed nuclei [25]:

$$\langle \ell^2(E) \rangle_{(i)} = \frac{\sum_{\ell=0}^{\ell=\ell_d} \ell^2 \langle \sigma_{(i)}^{(\ell)} \rangle_{\alpha_P, \alpha_T}(E)}{\sum_{\ell=0}^{\ell=\ell_d} \langle \sigma_{(i)}^{(\ell)} \rangle_{\alpha_P, \alpha_T}(E)} \tag{3}$$

with

$$\left\langle \sigma_{(i)}^{(\ell)} \right\rangle_{\{\alpha_P, \alpha_T\}}(E) = \int_0^{\pi/2} \sin \alpha_P \int_0^{\pi/2} \sin \alpha_T \times \sigma_{(i)}^{(\ell)}(E; \alpha_P, \alpha_T) \mathrm{d}\alpha_T \mathrm{d}\alpha_P, \tag{4}$$

where $i = fus$ or qf, and α_P and α_T are the orientation angles of the axial symmetry axes of the projectile and target nuclei, respectively.

The effective temperature T_{sad} at the saddle point is related to the excitation energy by the expression

$$T_{sad} = \left[\frac{E_{c.m.} + Q_{gg} - B_f(\ell) - E_n}{A_{CN}/8} \right]^{1/2}, \tag{5}$$

where Q_{gg} and $B_f(\ell)$ are the reaction Q_{gg}-value for the ground states of nuclei and the fission barrier height, respectively. The $B_f(\ell)$ is calculated in terms of the RFRM by Sierk [22]. For a given $E_{c.m.}$ we calculate $\langle \ell \rangle$ and its value is used to find $B_f(\ell)$. $A_{CN} = A_1 + A_2$ is the mass number of the composite system and E_n the energy carried away by the pre-saddle fission neutrons. The latter was not analyzed in this work. An important physical quantity in formula (1) is the variance K_0^2 of the Gaussian distribution of the K projection:

$$K_0^2 = \frac{\langle \mathcal{J}_{eff} T_{sad} \rangle}{\hbar^2}. \tag{6}$$

Often K_0 is used to fit the angular distribution of fission fragments (see ref. [5]).

Expression (1) can be used to calculate the anisotropy of the angular distribution of quasifission fragments due to the following reason which is similar to the case of fission: at quasifission, we have the dinuclear system in which the relative kinetic energy and mass distribution are

mainly relaxed; the quasifission barrier is considered as a saddle point for the dinuclear system. We can calculate all ingredients of expression (1) in our model.

For the estimation of the anisotropy of quasifission fragments, we calculate $\mathcal{J}_{eff}$ for the dinuclear system taking into account the possibility of different orientation angles of its constituent nuclei (see appendix A). The excitation energy of the dinuclear system is found as the sum of the difference between the beam energy and the minimum of the potential well of the interaction potential and the Q_{gg}-value corresponding to a change of the excitation energy of the dinuclear system from the projectile-target configuration to the quasifission fragments. Assuming that after capture the mutual orientations of the DNS nuclei do not change much, we calculate $\mathcal{J}_{eff}$ for collisions of the projectile and target with different time-independent orientations of their symmetry axes. Under this assumption, and using our calculated mean square values $\langle \ell^2 \rangle$ for quasifission, we determine the angular anisotropy A of the quasifission fragments. The effective value $\mathcal{J}_{eff}$ of the moment of inertia of the dinuclear system ($\mathcal{J}_{eff}^{(DNS)}$) is found by averaging on all the ℓ values and orientations (α_P, α_T) with the partial capture cross-sections, for a given collision energy:

$$\mathcal{J}_{eff}^{(DNS)} = \sum_{\alpha_P,\alpha_T} \sum_{\ell} \mathcal{J}^{(DNS)}(\ell, \alpha_P, \alpha_T) \sigma_{cap}^{(\ell)}(\alpha_P, \alpha_T) \Big/ \sum_{\alpha_P,\alpha_T} \sum_{\ell} \sigma_{cap}^{(\ell)}(\alpha_P, \alpha_T), \quad (7)$$

where $\sigma_{cap}^{(\ell)} = \sigma_{fus}^{(\ell)} + \sigma_{qf}^{(\ell)}$. The values of $\langle \ell^2 \rangle$ for the fragments of quasifission are higher than the ones of the compound nuclei [25]. This kind of fission-like decay produces a high anisotropy in the angular distributions due to the large angular momentum of DNS [26], because the partial cross-section of quasifission increases by increasing ℓ [25,27]. The reason is that the hindrance for the transformation of the dinuclear system into the compound nucleus increases due to an increase of the intrinsic fusion barrier B_{fus}^{*} with the orbital angular momentum ℓ. At the same time the quasifission barrier B_{qf} decreases by increasing ℓ [27,28]. We determine these barriers of the DNS model in sect. 4.2.

The dissipation of the initial orbital angular momentum ℓ_0 of collision during the capture process and the maximum value ℓ_d of the partial waves leading to capture are calculated by the solution of the corresponding equation of motion. The results show that such a dissipation is considerable and the value of angular momentum after dissipation ℓ_f is about 25–30% lower than the initial value ℓ_0. This value is found by the solution of the equations of motion for the orbital angular momentum and radial motion of nuclei. Details of these calculations can be found in refs. [25,29,30]. The possibility to calculate the spin distribution of the compound nucleus (its angular-momentum distribution) is the advantage of the used method based on the dinuclear-system concept [31]. In the next sect. 4.1 we shortly present the basic points of the model.

It should be stressed that, in the case of collisions of deformed nuclei, the orientation angles $(\alpha_{P,T})$ of the symmetry axes to the beam direction play an important role at the capture and complete-fusion stages. The importance of the orientation angles of the symmetry axes of the reacting nuclei was analyzed in ref. [25]. The final results of the capture and complete fusion are obtained by averaging the contributions calculated for different orientation angles of the symmetry axes of the reacting nuclei with formula (4).

4 Capture, fusion and quasifission cross-sections

At the early stage of the reaction with massive nuclei, the complete fusion of colliding nuclei has a very strong competition with the quasifission process which decreases the probability of the compound-nucleus formation. The fusion and quasifission are considered as a two-stage process [25,27,29]: i) the formation of a dinuclear system as a result of the capture of the projectile nucleus by the target nucleus; ii) the transition of the dinuclear system into the compound nucleus (complete fusion) as a special channel of its evolution. The other alternative way of the dinuclear-system evolution is quasifission. The quasifission is the decay of the dinuclear system without formation of the compound nucleus. Both processes can produce fragments with similar characteristics as total kinetic energy and mass distributions. The ratio of yields from both channels depends on the structure of the PES (see, for example, fig. 1a) which is different for the different total mass and charge numbers. In fig. 1, we present the PES calculated for reactions leading to ^{227}Pa. The probability of quasifission is determined by the relief of the PES of the dinuclear system calculated as a function of the relative distance and mass asymmetry. In fig. 1b, the curve connecting minimums of the valley on the PES is the driving potential as a function of the charge asymmetry of the DNS fragments. The cut of the PES for a given charge number is the nucleus-nucleus interaction potential $V(R)$. The curve in fig. 1c was calculated for the $^{19}\mathrm{F} + {}^{208}\mathrm{Pb}$ reaction. The size of the potential well is determined by the orbital angular momentum leading to capture and the depth of the potential well is the quasifission barrier B_{qf} for a given charge asymmetry. For the interacting deformed nuclei the PES depends on the orientation angles of the symmetry axes (see formula (9)).

4.1 Capture

The partial capture cross-section is determined by the capture probability $\mathcal{P}_{cap}^{(\ell)}(E)$ which means that the colliding nuclei are trapped into the well of the nucleus-nucleus potential after dissipation of a part of the initial kinetic energy and orbital angular momentum:

$$\sigma_{cap}^{(\ell)}(E, \alpha_1, \alpha_2) = \pi \lambda^2 \mathcal{P}_{cap}^{(\ell)}(E, \alpha_1, \alpha_2). \quad (8)$$

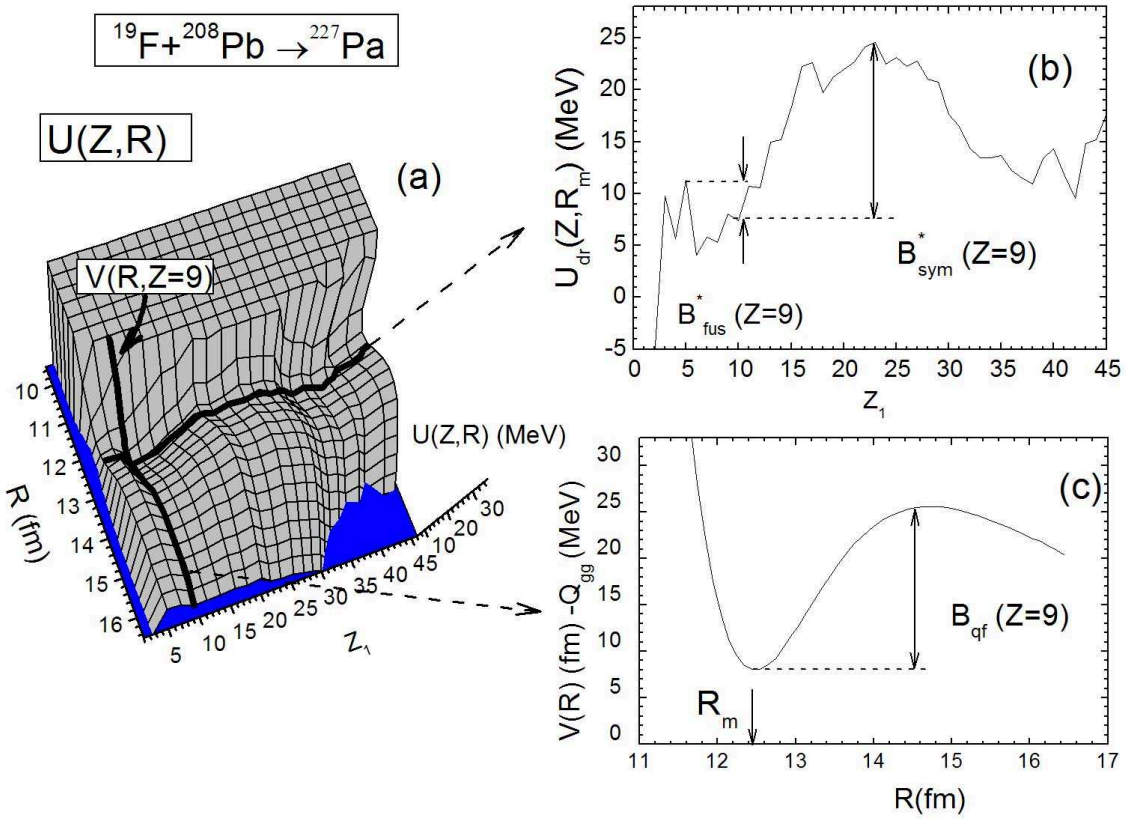

Fig. 1. (a) Potential energy surface for the reactions leading to ^{227}Pa as a function of the charge asymmetry of the dinuclear-system fragments and the relative distance between their centers. (b) Driving potential for the reactions leading to ^{227}Pa as a function of the charge asymmetry of the dinuclear-system fragments: the intrinsic fusion barrier B^*_{fus} is shown as the difference between the maximum value of the driving potential to the way of complete fusion and its value corresponding to the considered charge asymmetry of the entrance channel; the barrier to the mass symmetric configuration B^*_{sym} is shown as the difference between the maximum value of the driving potential to the way of symmetric masses and its value corresponding to the considered charge asymmetry of the entrance channel. (c) The nucleus-nucleus interaction potential $V(R)$ for the $^{19}\mathrm{F} + ^{208}\mathrm{Pb}$ system: the quasifission barrier B_{qf} as the a depth of the potential well.

Here $\lambda\!\!\!^{-}$ is the de Broglie wavelength of the entrance channel. The capture probability $\mathcal{P}^{(\ell)}_{cap}(E, \alpha_1, \alpha_2)$ is equal to 1 or 0 for given beam energy and orbital angular momentum. Our calculations showed that in dependence on the beam energy, $E = E_{c.m.}$, there is a window for capture as a function of orbital angular momentum (α_1 and α_2 are omitted here for the simplicity of the formula):

$$\mathcal{P}^{\ell}_{cap}(E) = \begin{cases} 1, & \text{if } \ell_m < \ell < \ell_d \text{ and } E > V_{Coul}\,, \\ 0, & \text{if } \ell > \ell_d \text{ or } \ell < \ell_m \text{ and } E > V_{Coul}\,, \\ 0, & \text{for all } \ell \quad \text{if } E \le V_{Coul}\,, \end{cases}$$

where $\ell_m \neq 0$ can be observed when the beam energy is larger than the Coulomb barrier (V_{Coul}). This means that the friction coefficient is not so strong to trap the projectile into the potential well (see fig. 2 in ref. [25]).

The number of partial waves giving a contribution to the capture is calculated by the solution of the equations for the radial and orbital motions simultaneously [29]. They are defined by the size of the potential well of the nucleus-nucleus potential $V(R, Z_1, Z_2; \{\beta^{(k)}_i\}, \{\alpha_k\})$ and the values of the radial γ_R and tangential γ_t friction coefficients, as well as by the moment of inertia for the relative motion. Here $Z_k, \beta^{(k)}_i$ and α_k are the charge numbers, deformation parameters and orientation angles of the symmetry axes of nuclei, $k = 1, 2$ and $i = 2, 3$ correspond to quadrupole and octupole deformations, respectively. The nucleus-nucleus interaction potential, radial and tangential friction coefficients and inertia coefficients are calculated in the framework of our model [25,27,29].

4.2 Complete fusion

For the capture events we calculate the competition between quasifission and complete fusion with a statistical approach [32]. The competition between the complete fusion and quasifission is obtained as the branching ratio between the transition of the dinuclear system from its position in the valley of the PES to the "fusion lake" overcoming the intrinsic fusion barrier B^*_{fus} on the charge number axis (complete fusion), and the decay to the "quasifission sea" after overcoming the quasifission barrier B_{qf}

on the radial distance axis. The size of the potential well decreases by increasing the orbital angular momentum ℓ, *i.e.* the valley of PES becomes shallow and as result the lifetime of the DNS decreases. At the same time the intrinsic fusion barrier B^*_{fus} increases while the quasifission barrier B_{qf} decreases. So, we conclude that the contribution of the quasifission increases by increasing the angular momentum for a given beam energy [27,28].

The intrinsic fusion barrier B^*_{fus} for a given projectile-target pair is the height of the saddle-point in the valley of the PES along the axis of the DNS charge asymmetry. The PES of the dinuclear system is calculated as the sum of the binding energies of interacting nuclei, the nucleus-nucleus interaction potential $V(R)$ and the rotational energy,

$$\begin{aligned} &U(Z,A,R,\{\beta_i^{(k)}\},\{\alpha_k\}) = Q_{gg} - V_{rot}^{CN}(\ell) \\ &+V(R,Z,Z_{CN}-Z;\{\beta_i^{(k)}\},\{\alpha_k\}) \\ &+V_{rot}^{(DNS)}(\ell,\{\beta_i^{(k)}\},\{\alpha_k\}), \end{aligned} \tag{9}$$

where $Q_{gg} = B_1(Z_1)+B_2(Z_{CN}-Z)-B_{CN}(Z_{CN})$, B_1, B_2, and B_{CN} are the binding energies of the constituent nuclei of the DNS and the compound nucleus, respectively; $Z_{CN} = Z_1 + Z_2$ and $V(R,Z,Z_{CN}-Z)$ is the nucleus-nucleus interaction potential of the DNS nuclei; $V_{rot}^{(DNS)}(\ell)$ and $V_{rot}^{CN}(\ell)$ are the rotational energies of DNS and the compound nucleus. $\beta_i^{(1,2)}$ and $\alpha_{1,2}$ are the deformation parameters and orientation angles of the axial symmetry axis of the interacting nuclei. The binding energy values are obtained from the tables in refs. [33,34]. The dependence of the PES on the shell structure of the nuclei forming the dinuclear system and on the orbital angular momentum leads to a strong influence of the entrance channel [25,27, 29,32].

The effects connected with the entrance channel appear in the partial fusion cross-section $\sigma_\ell^{fus}(E)$, which is defined by the product of the partial capture cross-section and the related fusion factor P_{CN} presenting the competition between complete fusion and quasifission processes:

$$\sigma^\ell_{fus}(E,\{\alpha_i\}) = \sigma^\ell_{cap}(E) P_{CN}(E,\ell,\{\alpha_i\}), \tag{10}$$

where $\sigma^\ell_{cap}(E)$ is the partial capture cross-section which is defined by formula (8). The details of the calculation method are described in ref. [32]. $P_{CN}(E,\ell)$ is the hindrance factor for formation of the compound nucleus connected with the competition between complete fusion and quasifission as possible channels of evolution of the DNS:

$$P_{CN}(E,\ell;\{\alpha_i\}) = \sum_{Z=Z_{sym}}^{Z_{max}} Y_Z(E^*_Z) P^{(Z)}_{CN}(E^*_Z,\ell;\{\alpha_i\}), \tag{11}$$

where

$$E^*_Z = E - V(Z,R_m,\ell;\{\beta_i\},\{\alpha_k\}) + \Delta Q_{gg}(Z) \tag{12}$$

is the excitation energy of the DNS for a given value of its charge-asymmetry configuration $(Z, Z_{CN}-Z)$; the position of the minimum value $V(Z,R_m,\ell;\{\beta_i\},\{\alpha_k\})$ of the nucleus-nucleus potential well is marked by $R = R_m$ (see fig. 1c); $\Delta Q_{gg}(Z)$ is the change of the Q_{gg}-value by changing the DNS charge asymmetry; $Y_Z(E^*_Z)$ is the population probability of the configuration $(Z, Z_{CN}-Z)$ at E^*_Z, ℓ and given orientation angles (α_P, α_T). $Y_Z(E^*_Z)$ was obtained by solving the master equation for the evolution of the dinuclear system (charge) mass asymmetry (for details see refs. [25,30]). $Z_{sym} = (Z_1 + Z_2)/2$ and Z_{max} correspond to the point where the driving potential reaches its maximum (see fig. 1b) [28,32].

The branching ratio $P^{(Z)}_{CN}(E^*_Z,\ell;\{\alpha_i\})$ is calculated as a ratio of the widths related to the overflowing over the quasifission barrier $B_{qf}(Z)$ at a given mass asymmetry, over the intrinsic barrier $B_{fus}(Z)$ on the mass asymmetry axis to complete fusion and over $B_{sym}(Z)$ in the opposite direction to the symmetric configuration of the DNS:

$$P^{(Z)}_{CN} \approx \frac{\Gamma_{fus}(Z)}{\Gamma_{qf}(Z)+\Gamma_{fus}(Z)+\Gamma_{sym}(Z)}. \tag{13}$$

Here, the complete-fusion process is considered as the evolution of the DNS along the mass asymmetry axis overcoming $B_{fus}(Z)$ (a saddle point between $Z = 0$ and $Z = Z_P$) and ending in the region around $Z = 0$ or $Z = Z_{CN}$ (fig. 1b). The evolution of the DNS in the direction of the symmetric configuration increases the number of events leading to the quasifission of more symmetric masses. This kind of channels is taken into account by the term $\Gamma_{sym}(Z)$. A similar way was used in ref. [35] in calculations of the evaporation residues cross-sections in reactions with actinides.

The widths of these "decays" leading to quasifission and complete fusion can be presented by the formula of the width of usual fission [36]:

$$\Gamma_i(Z) = \frac{\rho_i(E^*_Z)T_Z}{2\pi\rho(E^*_Z)}\left(1-\exp\frac{(B_i(Z)-E^*_Z)}{T_Z}\right), \tag{14}$$

where $\rho_i(E^*_Z) = \rho(E^*_Z - B_i(Z))$; $B_i = B_{fus}$, B_{qf}, and B_{sym}. T_Z is the temperature of the dinuclear system consisting of fragments with charge numbers Z and $Z_{CN}-Z$:

$$T_Z = \sqrt{8E^*_Z/A_{CN}}. \tag{15}$$

Usually, the value of the factor

$$(1-\exp[(B_i(Z)-E^*_Z)/T_Z])$$

in (14) is approximately equal to unity. Inserting eq. (14) in (13), we obtain the expression (16) used in our calculations:

$$P^{(Z)}_{CN}(E^*_Z) = \frac{\rho_{fus}(E^*_Z)}{\rho_{fus}(E^*_Z)+\rho_{qf}(E^*_Z)+\rho_{sym}(E^*_Z)}. \tag{16}$$

5 Results and discussion

In this section we compare the capture, fusion and quasifission excitation functions with the available experimental data which were obtained by the analysis of the angular distribution of fission fragments. The calculated partial capture, fusion and quasifission excitation functions in

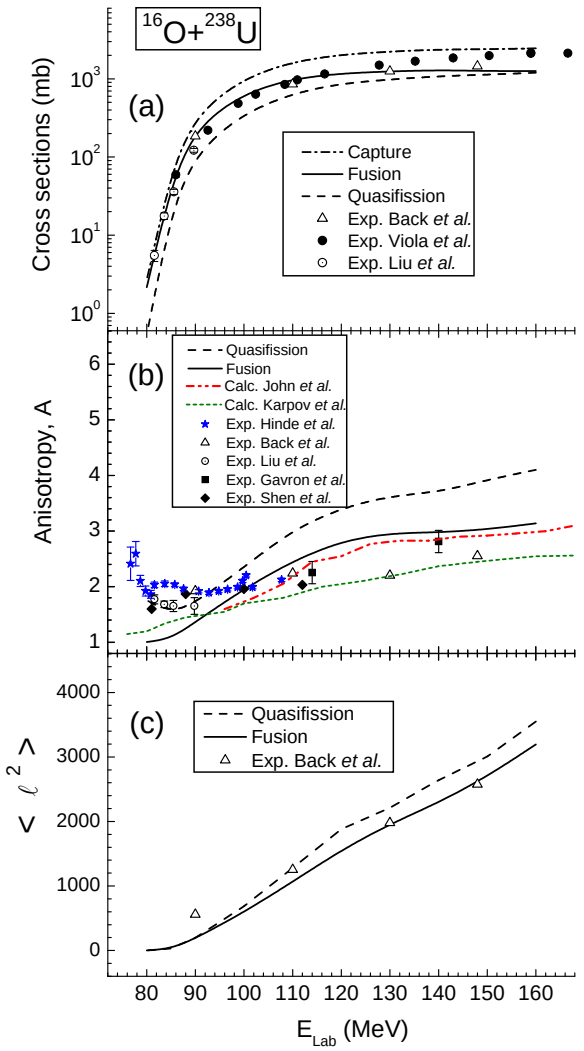

Fig. 2. (a) The calculated capture, fusion and quasifission excitation functions for the $^{16}\mathrm{O} + ^{238}\mathrm{U}$ reaction are compared with the measured fission excitation function of refs. [5,37,38]. (b) The anisotropy A of the angular distribution obtained in this work by the use of partial fusion and quasifission excitation functions is compared with the experimental data from refs. [4,5,7,38,39]. The results of calculations by the authors of refs. [15,19] for the anisotropy of fission products are presented by the double-dot-dashed and short-dashed curves, respectively. (c) The calculated values of $\langle \ell^2 \rangle$ for the $^{16}\mathrm{O} + ^{238}\mathrm{U}$ reaction obtained separately for complete fusion and quasifission in comparison with experimental data [5].

this work are used to determine the mean square values of the angular momentum $\langle \ell^2 \rangle$ for the dinuclear system and compound nucleus, and to find the anisotropy A of the angular distribution by formula (1). The results for A are compared with the experimental data.

Figure 2a shows that at low energies the calculated cross-sections are nearly equal and are in good agreement with the experimental data for the $^{16}\mathrm{O} + ^{238}\mathrm{U}$ reaction. The measured data is related by a mixture of the complete fusion and quasifission fragments in equal proportions. In

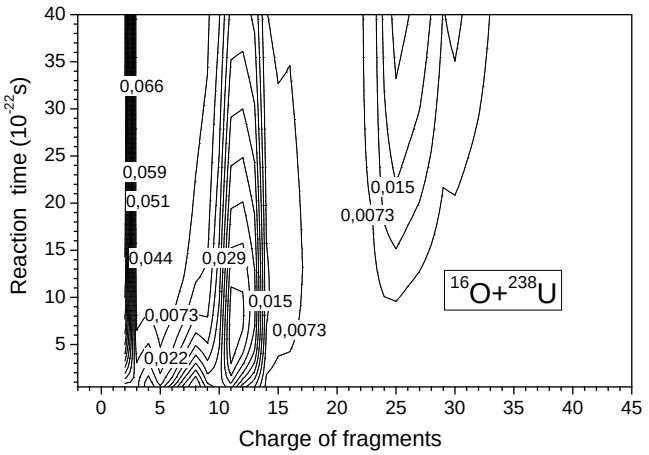

Fig. 3. The time dependence of the charge distribution of quasifission and deep inelastic nucleon transfer processes for the $^{16}\mathrm{O} + ^{238}\mathrm{U}$ reaction.

the energy interval $90 < E_{lab} < 130$ MeV the contribution of fragments of the fusion-fission process dominates over the one of quasifission (see fig. 2a). An increase of the quasifission contribution by increasing the beam energy is explained by the increase of events with the formation of the dinuclear system with large orbital angular momenta because the intrinsic fusion barrier B^*_{fus} increases and the quasifission barrier decreases by increasing ℓ (see refs. [25,28]).

The authors of ref. [7] analyzed in detail the angular anisotropy of fragments at low energies to show the dominant role of the quasifission in collisions of the projectile with the target nucleus when the axial symmetry axis of the latter is oriented along or near the beam direction. Large values of the anisotropy were obtained at low energies and these data were assumed to be connected with quasifission because a mononucleus or dinuclear system formed in the near tip collisions has an elongated shape. This shape can be far from the one corresponding to the saddle point [7]. Therefore, for such a system, there is a hindrance at its transformation into a compound nucleus.

The comparison of our calculated anisotropy values for the quasifission and complete-fusion fragments with the ones which were presented in refs. [5,7,37–39] shows that the anisotropy A connected with quasifission is very close to the experimental data (fig. 2b) at low energies $E_{lab} <$ 100 MeV. In spite of the fact that quasifission and fusion-fission cross-sections are close, the fusion-fission fragments show less anisotropy due to small $\langle \ell^2 \rangle$ values and large $\mathcal{J}_{eff}$. The large anisotropy for quasifission fragments is explained by small temperature T_{DNS} and small effective moment of inertia $\mathcal{J}^{(DNS)}_{eff}$. Because the fragments under discussion were formed in collisions with orientation angles $\alpha_T \leq 30^\circ$ for the target symmetry axis.

In fig. 3 we show the time dependence of the charge distribution $Y_Z(t)$ for the yield of the quasifission products in the $^{16}\mathrm{O} + ^{238}\mathrm{U}$ reaction. It was obtained by solving the master equation for the evolution of the dinuclear-system (charge) mass asymmetry (for details see ref. [25]). It is

seen that the light fragments of quasifission have charge numbers $Z = 12$ and 26 as asymptotic values. The maximum around $Z = 2$ and less corresponds to the complete fusion because in our calculations the smallest charge of a fragment is $Z = 2$. There is no contribution of quasifission fragments into the mass symmetric region. The corresponding heaviest fragments have a charge distribution around $Z = 88$ and 74. This result is caused by the influence of the shell structure of the interacting nuclei. Moreover, the fragments around the initial charge number $Z = 8$ at the reaction time $t = (5\text{–}10) \cdot 10^{-22}$ s can be considered as fragments of deep inelastic collisions when the dinuclear system is formed for the short times (no capture).

The results of the calculations by the authors of refs. [15] and [19] for the anisotropy of the fission products of the $^{16}O + ^{238}U$ reaction are presented in fig. 2b by the double-dot-dashed and short-dashed curves, respectively. They are in good agreement with the experimental data excluding the ones at the lowest beam energy. It is evident because these models have considered the experimental data for the angular anisotropy inherent to the pure fusion-fission products. The presence of quasifission products was not assumed. The increase of the anisotropy A at the lowest energies is inherent to quasifission products as was suggested by the authors of ref. [7] and our results have confirmed their statement.

Figure 2c shows the comparison of the calculated mean square of the angular momentum $\langle \ell^2 \rangle$ of the fissioning systems (dinuclear system and compound nucleus) with the data extracted from the measured angular distribution of fragments in ref. [5]. The agreement of the fusion and quasifission angular-momentum distributions with the experimental data is good for all values of the beam energy excluding the point $E_{lab} = 90$ MeV. The authors of ref. [40] concluded that in the sub-barrier region, in this reaction, the contribution of quasifission is negligible. This conclusion has been drawn by a comparison of calculated excitation functions for the evaporation residues with the experimental data [40]. The authors of [40] did not need to include a hindrance to fusion to reproduce the experimental data. The authors used the coupled-channel code CCDEGEN [41], which is based on a version of the CCFULL code described in [42] to calculate the fusion excitation function and the results were used as input for the statistical model calculation of evaporation residue cross-sections by using the code HIVAP [43].

One can see that even in the case of using a deformed target nucleus, at sub-barrier energies the yield of fusion-fission fragments is comparable with the yield of quasifission fragments. In fig. 4a, we show the comparison of the excitation functions for the capture, complete fusion and quasifission calculated for the $^{19}F + ^{208}Pb$ reaction in the framework of our model with the experimental data of the fission cross-sections presented in refs. [8,5,11]. Our results for the complete fusion are in agreement with the experimental data. This means that the contribution of quasifission in the measured data is small. We should note that the maximum of the calculated mass (charge) distribution of quasifission fragments is near the masses of the projectile-like and target-like fragments of the $^{19}F + ^{208}Pb$ reaction. The absence of a large anisotropy at low energies is explained by the fact that the massive target nucleus has a spherical shape and $\mathcal{J}_{eff}^{(DNS)}$ is not so small as in the $^{16}O + ^{238}U$ reaction.

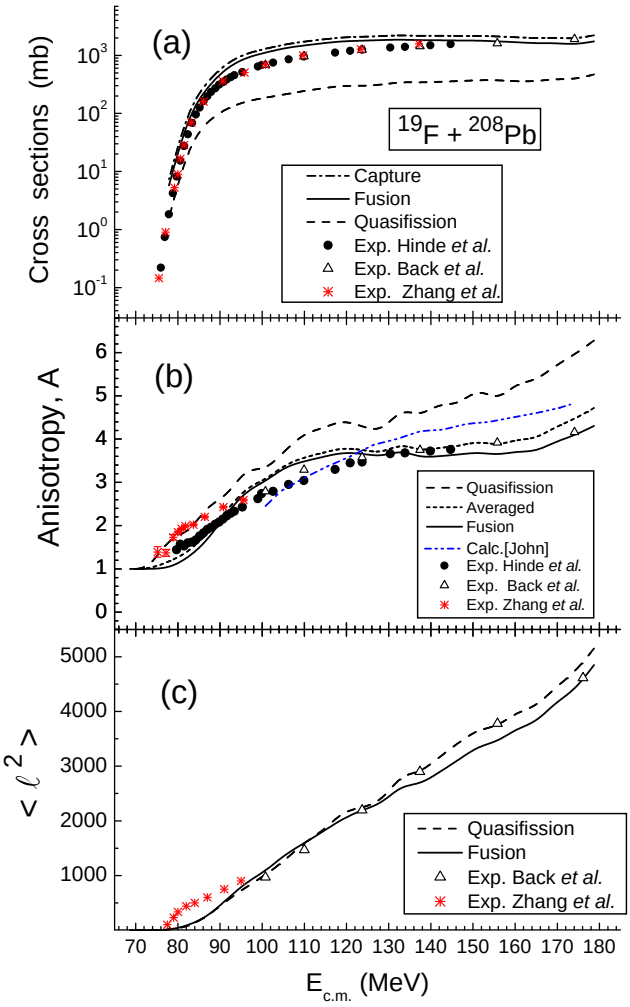

Fig. 4. (a) The calculated capture fusion and quasifission excitation functions for the $^{19}F + ^{208}Pb$ reaction are compared with the measured fission excitation function from refs. [5,8, 11]. (b) The anisotropy A of the angular distribution obtained in this work by the use of partial fusion and quasifission excitation functions is compared with the experimental data from refs. [5,8,11]. The results of calculations by the authors of ref. [15] for the anisotropy of fission products are presented by the double-dot-dashed curve. (c) Comparison of the values of $\langle \ell^2 \rangle$ for the $^{19}F + ^{208}Pb$ reaction calculated separately for the complete fusion and quasifission with the experimental data of refs. [5,11].

In fig. 5 we show the time dependence of the charge distribution $Y_Z(t)$ for the yield of the quasifission products. It is seen that the light fragments of quasifission have a charge less than $Z = 9$ and the asymptotic value is $Z = 5$. The heaviest fragments have a charge larger than $Z = 82$

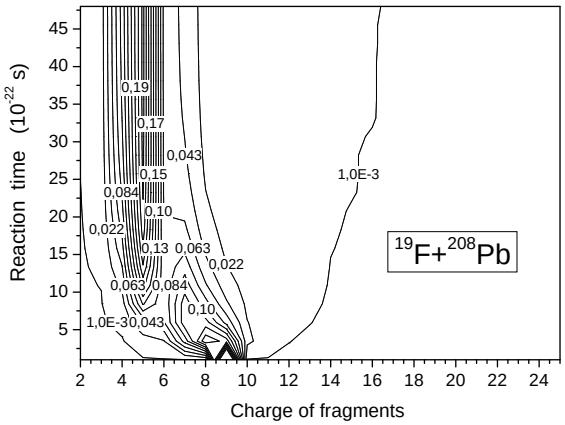

Fig. 5. The time dependence of the mass distribution of quasifission and deep-inelastic transfer processes for the $^{19}\mathrm{F} + ^{208}\mathrm{Pb}$ reaction.

and the largest value is $Z = 86$. This result is caused by the influence of the shell structure of the interacting nuclei. Moreover, the fragments around the initial charge number $Z = 9$ at a reaction time $t = (5\text{–}10) \cdot 10^{-22}$ s can be considered as fragments of deep inelastic collisions when the dinuclear system is formed for the short times (no capture).

From the good agreement of our results on the excitation function of the complete fusion and the angular anisotropy A for the $^{19}\mathrm{F} + ^{208}\mathrm{Pb}$ reaction (see fig. 4a and b) with the experimental data presented as the cross-section of the fusion-fission process, we can conclude that in this reaction the fusion-fission mechanism dominates over the quasifission mechanism. In fig. 4b, the results of calculations by the authors of ref. [15] for the anisotropy of the fission products of the $^{19}\mathrm{F} + ^{208}\mathrm{Pb}$ reaction are presented by the double-dot-dashed curve for comparison with our results and experimental data. It is seen that our results for the angular anisotropy of fusion-fission products are in good agreement with the experimental data and the results of ref. [15].

In fig. 4c our theoretical results are compared with the values of $\langle \ell^2 \rangle$ extracted from the description of the experimental results on the angular anisotropy A of the $^{19}\mathrm{F} + ^{208}\mathrm{Pb}$ reaction [5,11]. The good agreement between the calculated and experimental results confirms the correctness of the angular-momentum distribution for the complete fusion and quasifission calculated with our model.

The dominant role of quasifission can be seen in the $^{32}\mathrm{S} + ^{208}\mathrm{Pb}$ reaction which is more symmetric than the two above-discussed reactions. A sufficient role of the quasifission in this reaction was suggested by the authors of the experiment in ref. [5]. But they did not present quantitative results of the ratio between complete fusion and quasifission contributions. It is well known that this is a very complicated task due to the strong overlap in mass and angular distributions of the fragments from both processes.

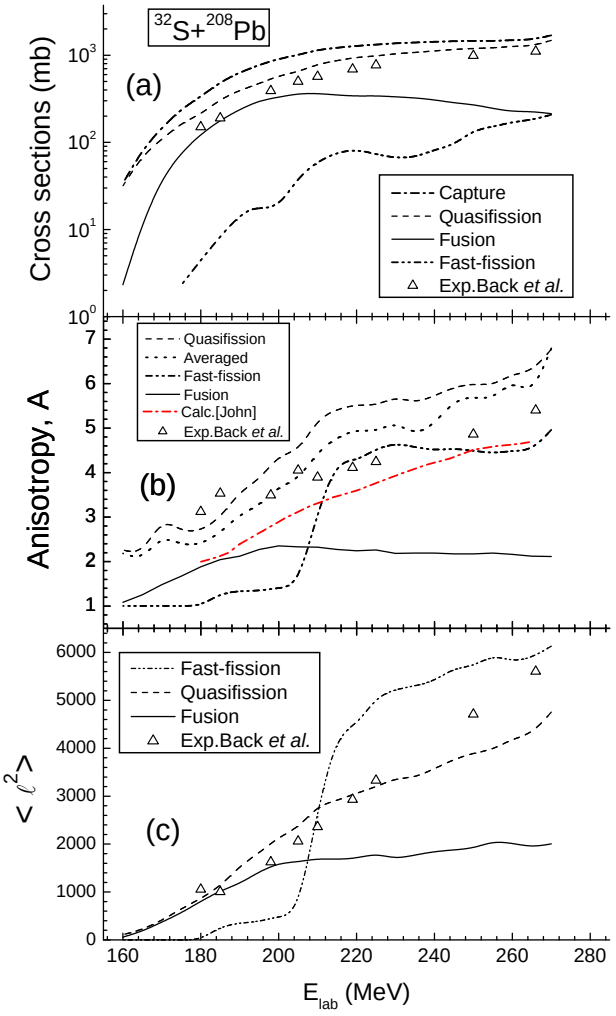

Fig. 6. (a) The calculated capture, fusion and quasifission excitation functions for the $^{32}\mathrm{S} + ^{208}\mathrm{Pb}$ reaction are compared with the measured fission excitation function of ref. [5]. (b) The anisotropy A of the angular distribution obtained in this work by using the partial fusion and quasifission excitation functions is compared with the experimental data of ref. [5]. The results of calculations by the authors of ref. [15] for the anisotropy of fission products are presented by the dot-dashed curve. (c) The values of $\langle \ell^2 \rangle$ for the $^{32}\mathrm{S} + ^{208}\mathrm{Pb}$ reaction calculated separately for the complete fusion and quasifission in comparison with the experimental data of ref. [5].

We have theoretically analyzed the contributions of the above-mentioned processes. In fig. 6a, we compare the excitation functions for capture, complete fusion and quasifission calculated for this reaction with the experimental data for the fission cross-section presented in ref. [5]. Our results for complete fusion are lower than the experimental fission cross-sections. Our statement is that the data contain a large amount of contributions of the quasifission fragments together with fusion-fission fragments. The ratio of the yields of quasifission fragments to fusion-fission fragments is larger at the lowest and highest beam energies. At the lowest energies the competition between

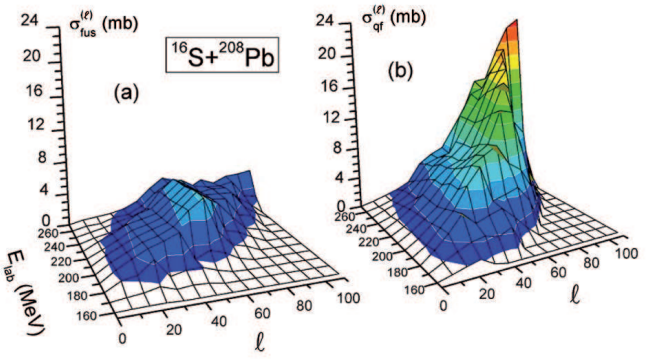

Fig. 7. Angular-momentum distribution of the partial cross-sections for (a) complete fusion and (b) quasifission calculated for the $^{32}\mathrm{S} + {}^{208}\mathrm{Pb}$ reaction.

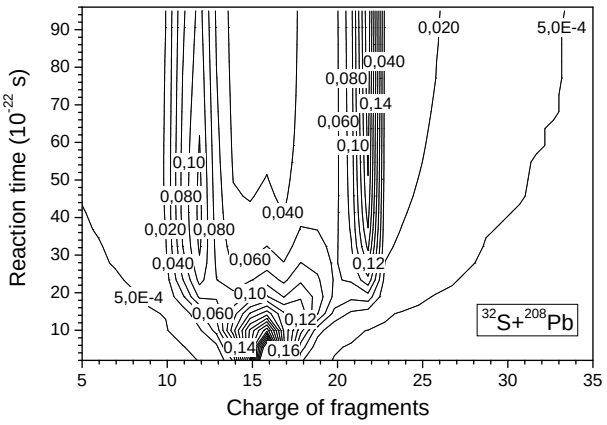

Fig. 8. The time dependence of the charge distribution of quasifission and deep inelastic transfer processes for the $^{32}\mathrm{S} + {}^{208}\mathrm{Pb}$ reaction.

complete fusion and quasifission is very sensitive to the peculiarities of the potential energy surface. The height of the intrinsic fusion barrier B^*_{fus} is comparable with the excitation energy of the dinuclear system and, therefore, there is a hindrance to complete fusion.

At the highest values of the beam energy the hindrance to complete fusion appears due to the increase of B^*_{fus} as a function of the orbital angular momentum ℓ_{DNS} of the dinuclear system. At the same time the quasifission barrier B_{qf} decreases by increasing ℓ_{DNS}. The combined effect from the behaviour of the B^*_{fus} and B_{qf} barriers as functions of ℓ_{DNS} makes quasifission the dominant process [27,28]. This phenomenon is common for all reactions with projectiles heavier than ^{16}O. The fast-fission mechanism also contributes to the anisotropy of the angular distributions of fragments in all of the above-mentioned reactions at large values of ℓ. According to its definition, the fast-fission mechanism takes place when complete fusion occurs at large orbital angular momentum but there is not a fission barrier for the compound nucleus being formed. The range of angular momentum leading to the fast fission is $\ell_{B_f=0} < \ell < \ell_{fus}$, where ℓ_{B_f} is the value at which the fission barrier for the compound nucleus disappear; ℓ_{fus} is the maximum value of ℓ at which complete fusion takes place. The value of ℓ_{fus} is different for different orientation angles of the colliding nuclei.

Note that quasifission can take place at small values of the angular momentum including $\ell = 0$ in contrast to the fast fission which occurs at $\ell_B \leq \ell \leq \ell_{cap}$ where ℓ_B is the minimum value of the angular momentum of the compound nucleus, where the fission barrier disappears and ℓ_{cap} is the maximum value of the orbital angular momentum leading to capture. In fig. 7, we present as an example our results of the angular-momentum distribution of the partial fusion and quasifission cross-sections for the $^{32}\mathrm{S} + {}^{208}\mathrm{Pb}$ reaction.

We estimated the contribution of the fast fission in the $^{32}\mathrm{S} + {}^{208}\mathrm{Pb}$ reaction. As fig. 6a shows, the fast-fission cross-section is small in comparison with the one of the other processes. At large beam energies, the fast-fission and complete-fusion cross-sections are comparable. The energy dependences of the anisotropy of the angular distribution of reaction fragments are shown in fig. 6b. The contribution of the fusion-fission process is small in comparison with the data from ref. [5]. This fact shows the dominance of quasifission fragments in the measured anisotropy of the angular distribution. This is the reason why the experimental data is underestimated by the theoretical results by the authors of ref. [15] for the anisotropy A, which are presented by the dot-dashed curve in fig. 6.

The dotted line in fig. 6b is obtained by averaging the anisotropies A_{qf}, A_{fus} and A_{ff} corresponding to the quasifission, fusion-fission and fast-fission fragments, respectively, according to the formula:

$$\langle A \rangle = \frac{(\sigma_{qf} A_{qf} + \sigma_{fus} A_{fus} + \sigma_{ff} A_{ff})}{(\sigma_{qf} + \sigma_{fus} + \sigma_{ff})}, \qquad (17)$$

where σ_{qf}, σ_{fus}, and σ_{ff} are the quasifission, fusion, and fast-fission cross-sections, respectively; A_{qf}, A_{fus}, and A_{ff} are the corresponding anisotropies. We would like to stress that the contribution of the fast-fission products A_{ff} is closer to the experimental data at the beam energies $E_{lab} > 210\,\mathrm{MeV}$. One can say that the role of fast fission becomes important at higher energies.

In fig. 6c, we compare our theoretical results with the values of $\langle \ell^2 \rangle$ extracted from the description of the experimental data on the angular anisotropy A of the $^{32}\mathrm{S} + {}^{208}\mathrm{Pb}$ reaction in ref. [5]. The extracted values of $\langle \ell^2 \rangle$ from the measured data are in good agreement with our theoretical results for the fusion-fission process. Note that at lower and higher values of the beam energy, the curve for the quasifission is closer to the experimental data. This confirms our conclusion of the role of quasifission made above in the discussion of fig. 6a.

In order to comment the overestimation of the measured data by our results for the quasifission excitation function, we calculated the evolution of the charge distribution in the dinuclear system as in the case of the $^{19}\mathrm{F} + {}^{208}\mathrm{Pb}$ reaction. The maximum of the charge distribution of the $^{32}\mathrm{S} + {}^{208}\mathrm{Pb}$ reaction splits into two peaks with increasing interaction time. It is seen from fig. 8 that

the first maximum of the lightest components is concentrated around the charge number $Z = 12$ and the other maximum around the charge value $Z = 22$. This effect is connected with the influence of the shell structure of the interacting nuclei. It seems to us that the quasifission fragments around $Z = 12$ were not registered as fission fragments. This is seen from fig. 6 of ref. [44]. But such fragments are included in our results of the quasifission contribution. As a result we overestimated the experimental data of refs. [5,44] for the yield of binary fragments of the full momentum transfer reactions.

The fragments around the initial charge number $Z = 16$ at time $t = (5\text{–}10)\cdot 10^{-22}$ s in fig. 8 can be considered as fragments of deep inelastic collisions when the dinuclear system is formed for a short time (no capture).

6 Dynamical calculation of the angular anisotropy of quasifission products

We present the results for the anisotropy A calculated by an alternative way for the quasifission fragments of the $^{16}\mathrm{O} + ^{238}\mathrm{U}$ reaction (see fig. 3) using the angular distribution of fragments and partial quasifission cross-sections to compare with the corresponding results obtained by the statistical method in the previous section.

The angular anisotropy for the quasifission products is defined by the ratio

$$A_{qf} = W_{qf}(0^\circ)/W_{qf}(90^\circ) \tag{18}$$

of their angular distribution $W_{qf}(\theta)$. The angular velocity and moment of inertia for the dinuclear system formed after capture for given beam energy and orbital angular momentum are known quantities from our calculation. The rotational angle of the dinuclear system during capture for given initial values of beam energy and orbital angular momentum L_0 is found by solving the equation of motions [29] for capture. If we neglect the decrease of the angular momentum of the dinuclear system by emission of light particles (gamma quanta, neutrons, etc.) during its evolution to quasifission, its angular momentum L_{DNS} can be considered as a constant value. We should note that L_{DNS} is less than the initial orbital angular momentum L_0 due to dissipation during capture. Its decrease is calculated by our model [29]. The knowledge of L_{DNS} and moment of inertia $J_{(DNS)}$ of the dinuclear system allows us to find its angular velocity Ω_{DNS}. At the considered beam energies, the dinuclear system is formed when the interacting nuclei are trapped into the potential well because the relative kinetic energy decreases due to the dissipation and it becomes not enough to overcome the quasifission barrier by the classical dynamical way. The characteristic lifetime of the DNS at quasifission is about or more than $5 \cdot 10^{-22}$ s. To find the angular distribution of the quasifission fragments, we estimate the rotational angle θ_{DNS} at the break-up of the system:

$$\theta_{DNS} = \theta_{cap} + \Omega_{DNS} \cdot \tau(T_Z(\ell, E^*_Z(\ell))). \tag{19}$$

It can be found if we know the decay time ($\tau(T_Z)$) of the rotated dinuclear system which is heated up to the effective temperature $T_Z(\ell, E^*_Z(\ell))$, where $E^*_Z(\ell)$ is the excitation energy of the DNS which is defined by expression (12). $T_Z(\ell, E^*_Z(\ell))$ is calculated by formula (15). The requested decay time τ is estimated by

$$\tau(T_Z) = \frac{\hbar}{\Gamma_{qf}(T_Z)}, \tag{20}$$

if we know the excitation energy E^*_{DNS} and the quasifission barrier B_{qf} of the dinuclear system for its decay to fragments with charge numbers Z and $Z_{tot} - Z$, by using the one-dimensional Kramers rate [45–47]

$$\Gamma_{qf}(\Theta) = K_{rot}\,\omega_m \left(\sqrt{\gamma^2/(2\mu_{qf})^2 + \omega^2_{qf}} - \gamma/(2\mu_{qf})\right) \times \exp\left(-B_{qf}/T_Z\right)\big)/(2\pi\omega_{qf}). \tag{21}$$

Here the frequencies ω_m and ω_{qf} are found by the harmonic-oscillator approximation to the nucleus-nucleus potential $V(R)$ shape for the given DNS configuration $(Z, Z_{tot} - Z)$ on the bottom of its pocket placed at R_m and on the top (quasifission barrier) placed at R_{qf} (see fig. 1c), respectively:

$$\omega^2_m = \mu^{-1}_{qf} \left|\frac{\partial^2 V(R)}{\partial R^2}\right|_{R=R_m}, \tag{22}$$

$$\omega^2_{qf} = \mu^{-1}_{qf} \left|\frac{\partial^2 V(R)}{\partial R^2}\right|_{R=R_{qf}}. \tag{23}$$

The calculated values of $\hbar\omega_m$ and $\hbar\omega_{qf}$ are equal to 46.52 MeV and 22.37 MeV, respectively. The used value of the friction coefficient γ is equal to $8 \cdot 10^{-22}$ MeV fm^{-2} s which was found from our calculations; $\mu_{qf} \approx \mu = A_1 \cdot A_2/A_{CN}$, where A_1 and A_2 are the mass numbers of the quasifission fragments.

The collective enhancement factor of the rotational motion K_{rot} to the level density should be included because the dinuclear system is a good rotator. It is calculated by the well-known expression [48]:

$$K_{rot}(E_{DNS}) = \begin{cases} (\sigma^2_\perp - 1) f(E_{DNS}) + 1, & \text{if } \sigma_\perp > 1\,, \\ 1, & \text{if } \sigma_\perp \le 1\,, \end{cases}$$

where $\sigma_\perp = J_{(DNS)}T/\hbar^2$; $f(E) = (1+\exp[(E-E_{cr})/d_{cr}])$; $E_{cr} = 120\widetilde{\beta}^2_2 A^{1/3}$ MeV; $d_{cr} = 1400\widetilde{\beta}^2_2 A^{2/3}$. $\widetilde{\beta}$ is the effective quadrupole deformation for the dinuclear system. We find it from the calculated $\mathcal{J}^{(DNS)}_\perp$.

The dinuclear system can be formed by different orientation angles of the symmetry axes of colliding nuclei (α_1 and α_2 with respect to the beam direction). Therefore, we perform all of these calculations for the different values of α_1 and α_2. The averaged values of the angular distribution $W_{qf}(\theta)$ is obtained by the assumption that the probability of the angular distribution for a given ℓ is equal to the corresponding value of the partial quasifission cross-section: $W_{qf}(\theta) = \sigma_{qf}(\ell)$, because θ is unambiguously determined by ℓ at given beam energy and orientation angles of nuclei.

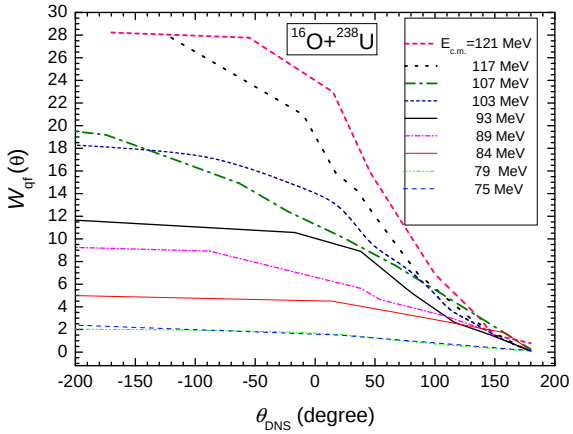

Fig. 9. The calculated probability of the angular distribution of quasifission fragments for the ^{16}O + ^{238}U reaction as a function of the rotational angle of the light fragment at decay of DNS for different beam energies.

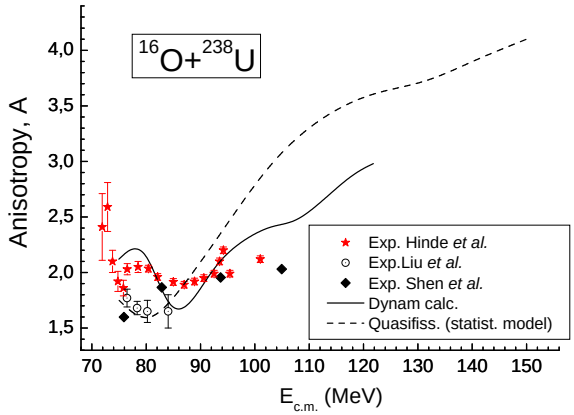

Fig. 10. The results of the anisotropy A of the angular distribution of the quasifission fragments for the ^{16}O + ^{238}U reaction calculated by dynamical method (solid line) is compared with the measured anisotropy for the fission fragments obtained from refs. [4,7,38] and with the result of the statistical calculations (dashed line) presented in fig. 2b by the dashed line.

The results of $W_{qf}(\theta)$ are presented in fig. 9. The results of dynamical calculations of the angular anisotropy A_{qf} which were found from the angular distribution are presented in fig. 10 (full line), and they are compared with the value of A_{qf} calculated by formula (1) (dashed line) and with the experimental data of the angular anisotropy A obtained in refs. [4,7,38].

The comparison of these results shows that our results obtained by the dynamical method are approximately in agreement with the results of the statistical calculations for the quasifission fragments and also with the measured anisotropy A in the $E_{c.m.} = 74$–102 MeV range where the yields of fusion-fission fragments are comparable with the yields of the quasifission fragments.

7 Conclusions

The model based on the dinuclear system [25,27,31] was improved to study the influence of the quasifission on the angular anisotropy of the measured fission-like fragments. We compared our calculated results with the experimental data on the excitation function of the fusion-fission process, the anisotropy A of the angular distributions of the fission fragments and mean square values $\langle \ell^2 \rangle$ extracted from the description of the measured anisotropy A for the ^{16}O + ^{238}U [5,7,37–39], ^{19}F + ^{208}Pb [5,8,11] and ^{32}S + ^{208}Pb [5] reactions. We explain the distinct deviation of the measured angular distributions of the fusion-fission reaction fragments by the presence of a contribution of the quasifission reactions.

The importance of the quasifission mechanism at the lowest beam energies was used to explain the large anisotropy of the angular distribution of fragments of the full momentum transfer reaction in ref. [8]. Our results obtained taking into account contributions of different orientation angles of the symmetry axis of the deformed ^{238}U target to the measured anisotropy A confirm this interpretation. At low beam energies we observe capture (formation of a relatively long-living DNS) only for $\alpha_T \leq 30^\circ$ and the angular distribution of the quasifission fragments shows large anisotropy, $A = 1.7$–2.0. The small values of $\mathcal{J}_{eff}^{(DNS)}$ and the DNS temperature T_{DNS} are responsible for this phenomenon. In the reactions with the spherical ^{208}Pb target, $\mathcal{J}_{eff}^{(DNS)}$ is not so small to cause in ^{19}F + ^{208}Pb an effect similar to that observed in the ^{16}O + ^{238}U reaction. The calculated fusion and quasifission cross-sections are nearly equal and are in good agreement with the experimental data for the ^{16}O + ^{238}U reaction. Therefore, we conclude that the measured data is related by a mixture of complete-fusion and quasifission fragments. The results of calculations by the authors of refs. [15] and [19] for the anisotropy of the fission products of the ^{16}O + ^{238}U reaction are in good agreement with the experimental data excluding the ones at the lowest beam energy. This is clear because these models have considered the experimental data for the angular anisotropy inherent to the pure fusion-fission products. The presence of quasifission products was not assumed in their models.

Considering the quasifission as a "fission" of the dinuclear system from a non-compact shape, we estimate the mean square values of the angular momentum ℓ and anisotropy A of the angular distribution of the reaction fragments. The experimental data of the anisotropy A are described if we also take into account the contribution of the quasifission fragments. This conclusion is also supported by the results of the dynamical calculations of the angular anisotropy A_{qf} of the quasifission products. The results of the angular anisotropy for the quasifission products is defined directly by the ratio $A_{qf} = W_{qf}(0^\circ)/W_{qf}(90^\circ)$ of their angular distribution $W_{qf}(\theta)$.

For the ^{19}F + ^{208}Pb reaction [5,8,11] the contribution of the quasifission fragments is comparable at low energies with the one of the fusion-fission mechanism and the last mechanism become dominant for the beam energy

$E_{lab} > 90$ MeV. So in the $^{19}F + ^{208}Pb$ reaction the fusion-fission fragments give the main contribution to the measured data. The comparison of our results for the angular anisotropy of fusion-fission products and the theoretical results of ref. [15] with the experimental data shows good agreement. The effect of quasifission appears only at higher beam energies.

The analysis of the measured data for the $^{32}S + ^{208}Pb$ reaction showed the dominant role of quasifission in this reaction. It was determined by the comparison of the calculated fusion and quasifission cross-sections, anisotropies A_{fus} and A_{qf} connected with these processes, as well as $\langle \ell^2 \rangle$ with the corresponding experimental data. In our opinion, the dominant role of quasifission in the $^{32}S + ^{208}Pb$ reaction is the reason why the experimental data was underestimated by the theoretical results by the authors of ref. [15] for the anisotropy A, since the model developed in ref. [15] devoted to describe the anisotropy of the pure fusion-fission products.

We would like to stress that the appearance of the competition between quasifission and complete fusion depends on such parameters of the entrance channel of reactions as mass asymmetry, orbital angular momentum and beam energy. Our experience showed that in reactions with massive nuclei or with less mass asymmetric reactions, quasifission occurs also at small values of the angular momentum.

This conclusion supports the statement of B. Back *et al.* [5] and M. Tsang *et al.* [44] that the assumption of fusion (and formation of a truly equilibrated compound nucleus) during the first step of the reaction is not valid in the analysis of the experimental data of fission fragments. Therefore, these authors hypothesized the quasifission contribution in the experimental data in order to describe the angular anisotropy of the detected fragments. The good agreement of our results with the experimental data shows that our model can be applied to analyze the anisotropy of the angular distribution of the reaction fragments and the contribution of quasifission fragments in the measured data which depend on the charge asymmetry of the reaction in the entrance channel, peculiarities of the shape and shell structure of colliding nuclei.

The authors are grateful to Profs. R.V. Jolos, A. Sobiczewski, and V.V. Volkov for helpful discussions. This work was performed partially under the financial support of the DFG, RFBR (Grant No. 04-02-17376) and INTAS (Grant 03-01-6417). The authors (AKN and RKU) thank DAAD and Polish-JINR cooperation Program for support while staying at the Giessen University and Soltan Institute for Nuclear Studies, respectively. AKN and RKU are also grateful to the Fondazione Bonino-Pulejo (FBP) of Messina for the support received in the collaboration with the Messina group. The authors (AIM, AKN and RKU) are grateful to the Center on Science and Technologies at the Ministry Cabinet (Grant No. F-2.1.8) and the Support Fund of Fundamental Research of the Academy of Science of Uzbekistan (No. 64-04) for partial support. A.K. Nasirov is grateful to the Université Libre de Bruxelles for the support received in the collaboration.

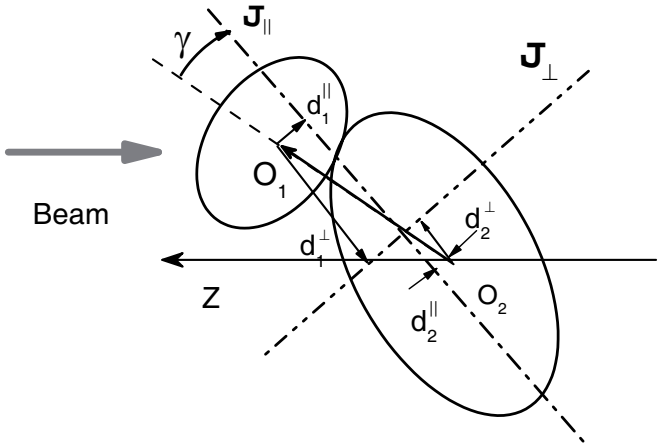

Fig. 11. The axes used to calculate the effective moment of inertia of the DNS.

Appendix A. Calculation of the effective moment of inertia $\mathcal{J}_{\mathrm{eff}}^{(\mathrm{DNS})}$ of the DNS

The effective moment of inertia $\mathcal{J}_{eff}^{(DNS)}$ of the DNS, which is formed in collisions of nuclei with the different orientation angles of their symmetry axes relative to the beam direction, is calculated by the formula (2). But the moments of inertia $\mathcal{J}_{\parallel}^{(DNS)}$ and $\mathcal{J}_{\perp}^{(DNS)}$ should be the smallest and largest components, respectively. The axis for which the value of $\mathcal{J}_{\parallel}$ is minimal is found from the condition $\frac{\partial \mathcal{J}_{\parallel}}{\partial \gamma} = 0$ (γ is the angle between the axis $\mathcal{J}_{\parallel}$ and the vector connecting the centers of masses O_1 and O_2 of the two interacting nuclei) (fig. 11). The $\mathcal{J}_{\perp}$-axis is directed as a normal to the reaction plane. The moments of inertia of nuclei are calculated as for a rigid-body system. For a quadrupole deformed nucleus the moment of inertia is calculated by the expression

$$\mathcal{J}_i = \frac{M_i}{5}(a_i^2 + c_i^2) \qquad i = 1, 2, \tag{A.1}$$

where a_i and c_i are the small and large semi-axes, respectively, of the DNS constituents ($i = 1, 2$).

The moments of inertia $\mathcal{J}_{\parallel}^{(DNS)}$ and $\mathcal{J}_{\perp}^{(DNS)}$ are found by using Steiner's theorem for the rigid-body moments of inertia of the DNS constituents:

$$\mathcal{J}_{\parallel}^{(DNS)} = \mathcal{J}_1 + \mathcal{J}_2 + M_1 d_{\parallel}^{(1)2} + M_2 d_{\parallel}^{(2)2}, \tag{A.2}$$

$$\mathcal{J}_{\perp}^{(DNS)} = \mathcal{J}_1 + \mathcal{J}_2 + M_1 d_{\perp}^{(1)2} + M_2 d_{\perp}^{(2)2}, \tag{A.3}$$

where $d_{\perp}^{(i)}$ ($d_{\parallel}^{(i)}$) is the distance between the center of mass of the fragment i ($i = 1, 2$) and the axis corresponding to the largest (smallest) moment of inertia of the dinuclear system.

References

1. Yu. Ts. Oganessian *et al.*, Phys. Rev. C **70**, 064609 (2004).

2. M.G. Itkis *et al.*, Nucl. Phys. A **734**, 136147 (2004).
3. G. Fazio, G. Giardina, A. Lamberto, A.I. Muminov, A.K. Nasirov, F. Hanappe, L. Stuttgé, Eur. Phys. J. A **22**, 75 (2004).
4. W.Q. Shen *et al.*, Phys. Rev. C **36**, 115 (1987).
5. B.B. Back *et al.*, Phys. Rev. C **32**, 195 (1985)
6. A. Diaz-Torres, Phys. Rev. C **74**, 064601 (2006).
7. D.J. Hinde, M. Dasgupta, J.R. Leigh, J.C. Mein, C.R. Morton, J.O. Newton, H. Timmers, Phys. Rev. C **53**, 1290 (1996).
8. D.J. Hinde, A.C. Berriman, M. Dasgupta, J.R. Leigh, J.C. Mein, C.R. Morton, J.O. Newton, Phys. Rev. C **60**, 054602 (1999).
9. B.B. Back *et al.*, Phys. Rev. Lett. **50**, 818 (1983).
10. R. Vandenbosch, J.R. Huizenga, *Nuclear Fission* (Academic, New York, 1973).
11. H. Zhang, Z. Liu, J. Xu, K. Xu, J. Lu, M. Ruan, Nucl. Phys. A **512**, 531 (1990).
12. H. Zhang, Z. Liu *et al.*, J. Nucl. Radiochem. Sci. **3**, 99 (2002).
13. H. Rossner, J.R. Huizenga, W.U. Schröder, Phys. Rev. C **33**, 560 (1986).
14. R. Freifelder, M. Prakash, J.M. Alexander, Phys. Rep. **133**, 315 (1986).
15. B. John, S.K. Kataria, Phys. Rev. C **57**, 1337 (1998).
16. V.S. Ramamurtby, S.S. Kapoor, Phys. Rev. Lett. **54**, 178 (1985); Phys. Rev. C **32**, 2182 (1985).
17. D. Vopkapić, B. Ivanišević, Phys. Rev. C **52**, 1980 (1995).
18. J. Tõke *et al.*, Nucl. Phys. A **440**, 327 (1985).
19. A.V. Karpov, R.M. Hiryanov, A.V. Sagdeev, G.D. Adeev, J. Phys. G: Nucl. Part. Phys. **34**, 255 (2007).
20. V.A. Drozdov, D.O. Eremenko, O.V. Fotina, G. Giardina, F. Malaguti, S.Yu. Platonov, O.A. Yuminov, Nucl. Phys. A **734**, 225 (2004).
21. V.A. Drozdov, D.O. Eremenko, S.Yu. Platonov, O.V. Fotina, O.A. Yuminov, Phys. At. Nucl. **64**, 179 (2001) (Yad. Fiz. **64**, 221 (2001)).
22. A.J. Sierk, Phys. Rev. C **33**, 2039 (1986).
23. I. Halpern, V.M. Strutinski, *Proceedings of the Second United Nations International Conference on the Peaceful Uses of Atomic Energy, Geneva, 1958*, Vol. **15** (United Nations, Geneva, 1958) p. 408.
24. J.J. Griffin, Phys. Rev. **116**, 107 (1959).
25. A.K. Nasirov *et al.*, Nucl. Phys. A **759**, 342 (2005).
26. T. Murakami, C.-C. Sahm, R. Vandenbosch, D.D. Leach, A. Ray, M.J. Murphy, Phys. Rev. C **34**, 1353 (1986).
27. G. Fazio *et al.*, Eur. Phys. J. A **19**, 89 (2004).
28. G. Fazio *et al.*, Phys. Rev. C **72**, 064614 (2005).
29. G. Giardina *et al.*, Eur. Phys. J. A **8**, 205 (2000).
30. A.K. Nasirov, G. Giardina, A.I. Muminov, W. Scheid, U.T. Yakhshiev, *Proceedings of the Symposium on Nuclear Clusters: from Light Exotic to Superheavy Nuclei, Rauischholzhausen, Germany, 5-9 August, 2002*, edited by R. Jolos, W. Scheid (EP Systema, Debrecen, Hungary, 2003) pp. 415–426; Acta Phys. Hungarica A **19**, 109 (2004).
31. V.V. Volkov, *Contributed Papers of Nucleus-Nucleus Collison II, Visby, 1985*, edited by B. Jakobson, K. Aleclett, Vol. **1** (North-Holland, Amsterdam, 1985) p. 54; Izv. Akad. Nauk SSSR Ser. Fiz. **50**, 1879 (1986); *Proceedings of the International School-Seminar on Heavy Ion Physics, Dubna, 1986*, D7-87-68 (Dubna, 1987) p. 528; *Proceedings of the 6th International Conference on Nuclear Reaction Mechanisms, Varenna, 1991*, edited by E. Gadioli, Supplemento n. 84 (Ricerca Scientifica ed Educazione Permanente, 1991) p. 39.
32. G. Fazio *et al.*, Mod. Phys. Lett. A **20**, 391 (2005).
33. G. Audi, A.H. Wapstra, Nucl. Phys. A **595**, 409 (1995).
34. P. Moller, J.R. Nix, W.D. Myers, W.J. Swiatecki, At. Data Nucl. Data Tables **59**, 185 (1995).
35. G.G. Adamian, N.V. Antonenko, W. Scheid, Phys. Rev. C **69**, 044601 (2004).
36. P.J. Siemens, A.S. Jensen, *Elements of Nuclei, Lecture Notes and Supplements in Physics* (Addison-Wesley, Redwood City, California, 1987).
37. V.E. Viola, T. Sikkeland, Phys. Rev. **128**, 767 (1962).
38. Z. Liu, H. Zhang, J. Xu, Yu Qiao, X. Qian, C. Lin, Phys. Rev. C **54**, 761 (1996).
39. A. Gavron *et al.*, Phys. Rev. Lett. **52**, 589 (1983).
40. K. Nishio, H. Ikezoe, Y. Nagame, M. Asai, K. Tsukada, S. Mitsuoka, K. Tsuruta, K. Satou, C.J. Lin, T. Ohsawa, Phys. Rev. Lett. **93**, 162701 (2004).
41. K. Hagino, unpublished.
42. K. Hagino, N. Rowley, A.T. Kruppa, Comput. Phys. Commun. **123**, 143 (1999).
43. W. Reisdorf, M. Schädel, Z. Phys. A **343**, 47 (1992).
44. M.B. Tsang, D. Ardouin, C.K. Gelbke, W.G. Lynch, Z.R. Xu, B.B. Back, R. Betts, S. Saini, P.A. Baisden, M.A. McMahan, Phys. Rev. C **28**, 747 (1983).
45. H.A. Kramers, Physica **7**, 284 (1940); V.M. Strutinsky, Phys. Lett. B **47**, 121 (1973).
46. P. Grangé *et al.*, Phys. Rev. C **27**, 2063 (1983); P. Grangé, Nucl. Phys. A **428**, 37c (1984).
47. P. Fröbrich, G.R. Tillack, Nucl. Phys. A **540**, 353 (1992).
48. A.R. Junghans, M. de Jong, H.-G. Clerc, A.V. Ignatyuk, G.A. Kudyaev, K.-H. Schmidt, Nucl. Phys. A **629**, 635 (1998).